AIAA 81-0049R

Numerical Solution of Supersonic Viscous Flow over Blunt Delta Wings

J. C. Tannehill* and Ethiraj Venkatapathy†
Iowa State University, Ames, Iowa
and
John V. Rakich‡
NASA Ames Research Center, Moffett Field, Calif.

A general parabolized Navier-Stokes code has been developed to compute the steady supersonic viscous flow around arbitrary body shapes at high angles of attack. A nonorthogonal three-dimensional coordinate frame is employed which permits the code to march with solution surfaces that are the most appropriate for a given problem. The code has been used to calculate the laminar flow over a slab delta wing with 70-deg sweep at angles of attack up to 41.5 deg and Mach numbers of 6.8 and 9.6. The computed shock shapes, surface pressures, and heat transfer coefficients are compared with experiment and show excellent agreement.

Introduction

THE "parabolized" Navier-Stokes (PNS) equations have been used to successfully compute the three-dimensional supersonic viscous flow over a variety of body shapes at angle of attack. These body shapes include pointed cones,[1-5] sphere cones,[6,7] hemisphere cylinders,[8] ogive cylinders,[9] ogive-cylinder boattails,[10] sharp leading-edge delta wings,[4] and blunt biconics.[11] Numerous additional applications have been made that demonstrate the usefulness of the PNS equations for a definable class of supersonic flows.

In order to apply the PNS equations, the inviscid region of the flow must be supersonic and the streamwise velocity component cannot be negative (i.e., only cross-flow separation is permitted). If these conditions are met, the PNS equations can be used to compute a flowfield at a fraction of the computer cost required to solve the complete time-dependent Navier-Stokes equations. In addition, viscous-inviscid interaction problems which have plagued boundary-layer methods are eliminated with the PNS equations.

Most of the previous applications of the PNS equations are limited to conical or axisymmetric body shapes. This is partly due to the fact that nearly all of the PNS codes are restricted to certain geometries by the coordinate systems employed. In the present study, a generalized PNS code has been developed which can be used to solve the steady supersonic viscous flow around any geometry for which the aforementioned Mach number and velocity conditions are met. This generalized code is an extension of the PNS code developed originally by Vigneron et al.[4] The previous code advances the solution on axis-normal surfaces which allows for most body geometries. However, for blunted bodies with large surface slope, the axial component of velocity in the inviscid part of the shock layer may be subsonic which prevents the code from computing this case. It was necessary, therefore, to generalize the code to march with solution surfaces that are more nearly normal to the local body surface. This has been done in a perfectly general manner with a nonorthogonal three-dimensional coordinate frame. The present approach is more flexible than the cited methods that use either axis-normal systems or strictly orthogonal coordinates in conjunction with surface normals.

The present generalized PNS code has been used to calculate the laminar flow over a slab delta wing with 70-deg sweep at angles of attack up to 41.5 deg and Mach numbers of 6.8 and 9.6. The computed results are compared with the experimental results[12] in this paper.

Governing Equations

The Navier-Stokes equations for an unsteady three-dimensional flow without body forces or external heat addition can be written in nondimensional, conservation-law form for a Cartesian coordinate system as

$$\frac{\partial U}{\partial t}+\frac{\partial (E-E_v)}{\partial x}+\frac{\partial (F-F_v)}{\partial y}+\frac{\partial (G-G_v)}{\partial z}=0 \tag{1}$$

where

$$U=\begin{bmatrix}\rho\\ \rho u\\ \rho v\\ \rho w\\ \rho e_t\end{bmatrix} \tag{2}$$

$$E=\begin{bmatrix}\rho u\\ \rho u^2+p\\ \rho uv\\ \rho uw\\ (\rho e_t+p)u\end{bmatrix} \qquad E_V=\begin{bmatrix}0\\ \sigma_{xx}\\ \tau_{xy}\\ \tau_{xz}\\ u\sigma_{xx}+v\tau_{xy}+w\tau_{xz}+q_x\end{bmatrix} \tag{3}$$

Presented as Paper 81-0049 at the AIAA 19th Aerospace Sciences Meeting, St. Louis, Mo., Jan. 12-15, 1981; submitted March 10, 1981; revision received July 20, 1981.

*Professor, Dept. of Aerospace Engineering and Computational Fluid Dynamics Institute. Associate Fellow AIAA.

†Research Assistant, Dept. of Aerospace Engineering and Computational Fluid Dynamics Institute.

‡Research Scientist. Associate Fellow AIAA.

$$F=\begin{bmatrix}\rho v\\ \rho uv\\ \rho v^2+p\\ \rho vw\\ (\rho e_t+p)v\end{bmatrix} \quad F_V=\begin{bmatrix}0\\ \tau_{xy}\\ \sigma_{yy}\\ \tau_{yz}\\ u\tau_{xy}+v\sigma_{yy}+w\tau_{yz}+q_y\end{bmatrix} \tag{4}$$

$$G=\begin{bmatrix}\rho w\\ \rho uw\\ \rho vw\\ \rho w^2+p\\ (\rho e_t+p)w\end{bmatrix} \quad G_V=\begin{bmatrix}0\\ \tau_{xz}\\ \tau_{yz}\\ \sigma_{zz}\\ u\tau_{xz}+v\tau_{yz}+w\sigma_{zz}+q_z\end{bmatrix} \tag{5}$$

$$e_t=e+\frac{u^2+v^2+w^2}{2} \tag{6}$$

and

$$\sigma_{xx}=\frac{2\mu}{3Re_L}\left(2\frac{\partial u}{\partial x}-\frac{\partial v}{\partial y}-\frac{\partial w}{\partial z}\right)$$

$$\sigma_{yy}=\frac{2\mu}{3Re_L}\left(2\frac{\partial v}{\partial y}-\frac{\partial u}{\partial x}-\frac{\partial w}{\partial z}\right)$$

$$\sigma_{zz}=\frac{2\mu}{3Re_L}\left(2\frac{\partial w}{\partial z}-\frac{\partial u}{\partial x}-\frac{\partial v}{\partial y}\right) \quad \tau_{xy}=\frac{\mu}{Re_L}\left(\frac{\partial u}{\partial y}+\frac{\partial v}{\partial x}\right)$$

$$\tau_{xz}=\frac{\mu}{Re_L}\left(\frac{\partial u}{\partial z}+\frac{\partial w}{\partial x}\right) \quad \tau_{yz}=\frac{\mu}{Re_L}\left(\frac{\partial v}{\partial z}+\frac{\partial w}{\partial y}\right)$$

$$q_x=\frac{\mu}{(\gamma-1)M_\infty^2 Re_L Pr}\frac{\partial T}{\partial x} \quad q_y=\frac{\mu}{(\gamma-1)M_\infty^2 Re_L Pr}\frac{\partial T}{\partial y}$$

$$q_z=\frac{\mu}{(\gamma-1)M_\infty^2 Re_L Pr}\frac{\partial T}{\partial z} \tag{7}$$

These equations have been nondimensionalized as follows (dimensional quantities are denoted by a tilde):

$$x=\tilde{x}/\tilde{L} \quad y=\tilde{y}/\tilde{L} \quad z=\tilde{z}/\tilde{L} \quad t=\tilde{t}/(\tilde{L}/\tilde{V}_\infty)$$

$$u=\tilde{u}/\tilde{V}_\infty \quad v=\tilde{v}/\tilde{V}_\infty \quad w=\tilde{w}/\tilde{V}_\infty \quad e=\tilde{e}/\tilde{V}_\infty^2$$

$$\rho=\tilde{\rho}/\tilde{\rho}_\infty \quad p=\tilde{p}/\tilde{\rho}_\infty\tilde{V}_\infty^2 \quad T=\tilde{T}/\tilde{T}_\infty \quad \mu=\tilde{\mu}/\tilde{\mu}_\infty \tag{8}$$

where $\tilde{L}$ is the reference length used in the Reynolds number

$$Re_L=\tilde{\rho}_\infty\tilde{V}_\infty\tilde{L}/\tilde{\mu}_\infty \tag{9}$$

In order to close the system of equations, the following perfect gas equations of state are used:

$$p=(\gamma-1)\rho e \qquad T=\gamma M_\infty^2 p/\rho \tag{10}$$

and the coefficient of viscosity μ is determined from Sutherland's equation

$$\mu=T^{3/2}\left(\frac{1+C}{T+C}\right) \tag{11}$$

where $C=110.4\,K/\tilde{T}_\infty$ for air.

In the previous version of the code,[4] a transformation of the form

$$\xi=\xi(x) \qquad \eta=\eta(x,y,z) \qquad \zeta=\zeta(x,y,z) \tag{12}$$

was used to transform the governing equations into the (ξ,η,ζ) system. This transformation restricts the (η,ζ) solution surfaces to be in a plane normal to the x axis and thereby limits the flowfields that can be computed with the code. In the new version of the code, a completely general transformation of the form

$$\xi=\xi(x,y,z) \qquad \eta=\eta(x,y,z) \qquad \zeta=\zeta(x,y,z) \tag{13}$$

is used which places no restrictions on the orientation of the (η,ζ) solution surfaces. When this transformation is applied to Eq. (1) the following conservation-law form[13] is obtained:

$$\frac{\partial\bar{U}}{\partial t}+\frac{\partial}{\partial\xi}\left\{\frac{1}{J}\left[\xi_x(E-E_v)+\xi_y(F-F_v)+\xi_z(G-G_v)\right]\right\}$$

$$+\frac{\partial}{\partial\eta}\left\{\frac{1}{J}\left[\eta_x(E-E_v)+\eta_y(F-F_v)+\eta_z(G-G_v)\right]\right\}$$

$$+\frac{\partial}{\partial\zeta}\left\{\frac{1}{J}\left[\zeta_x(E-E_v)+\zeta_y(F-F_v)+\zeta_z(G-G_v)\right]\right\}=0 \tag{14}$$

where

$$\bar{U}=U/J \tag{15}$$

and J is the Jacobian of the transformation which can be evaluated from

$$J=1/[x_\xi(y_\eta z_\zeta-y_\zeta z_\eta)-x_\eta(y_\xi z_\zeta-y_\zeta z_\xi)+x_\zeta(y_\xi z_\eta-y_\eta z_\xi)] \tag{16}$$

The parabolized Navier-Stokes equations are derived from the complete Navier-Stokes equations by assuming 1) steady flow ($\partial/\partial t\equiv 0$) and 2) streamwise viscous derivatives are negligible compared to normal and circumferential viscous derivatives [$\partial/\partial\xi$(viscous terms)$\cong 0$]. With these assumptions, Eq. (14) reduces to

$$\frac{\partial\bar{E}}{\partial\xi}+\frac{\partial\bar{F}}{\partial\eta}+\frac{\partial\bar{G}}{\partial\zeta}=0 \tag{17}$$

where

$$\bar{E}=(1/J)(\xi_x E+\xi_y F+\xi_z G)$$

$$\bar{F}=(1/J)[\eta_x(E-E_v)+\eta_y(F-F_v)+\eta_z(G-G_v)]$$

$$\bar{G}=(1/J)[\zeta_x(E-E_v)+\zeta_y(F-F_v)+\zeta_z(G-G_v)] \tag{18}$$

and terms in E_v, F_v, and G_v containing partial derivatives with respect to ξ are omitted.

As mentioned previously, the above system of equations is parabolized in the ξ direction if the inviscid region of the flow is supersonic and if the streamwise velocity component is positive. However, it has been shown[14] that an exact representation of the streamwise pressure gradient term $\partial p/\partial\xi$, causes information to be propagated upstream through the subsonic boundary layer close to the wall so that a marching method of solution is not well-posed. This leads to exponentially growing solutions that are often called departure solutions. A number of different techniques have been proposed to eliminate this difficulty. Lin and Rubin[5] recently compared these techniques while proposing a new

one. The obvious technique is to drop completely the pressure gradient term in subsonic regions. This will produce a stable marching scheme but will introduce errors in flowfields with large streamwise pressure gradients. In several studies[1-3,6,7,11] $\partial p/\partial \xi$ is retained in the subsonic layer by employing an approximate backward difference formula which can be extrapolated from the previous step. The eigenvalue stability analyses of Refs. 2 and 15 indicate this approach is subject to instabilities if the streamwise step $\Delta\xi$ is too small. Rubin and Lin[16] originally proposed the so-called "sublayer approximation" technique in which the pressure gradient term in the subsonic region is calculated at a supersonic point outside the sublayer region. This approximation is based on the fact that for a thin subsonic viscous layer, $\partial p/\partial \eta$ is negligible. The sublayer approximation technique is used in the code of Schiff and Steger.[8] Note, however, that the method originally employed by Rubin and Lin is essentially different in that the boundary-layer equations were solved in the sublayer. Schiff and Steger's sublayer approximation technique is explained further after the next paragraph.

A novel technique for handling the pressure gradient term was proposed by Vigneron et al.[4,15] In this approach, a fraction of the pressure gradient term $\omega(\partial p/\partial \xi)$ is retained in the subsonic viscous region and the remainder $(1-\omega)\partial p/\partial \xi$ is separated out and evaluated outside the subsonic region as in the sublayer approximation technique. An eigenvalue stability analysis indicates that for stability

$$\omega < \frac{\gamma M_\xi^2}{1+(\gamma-1)M_\xi^2} \tag{19}$$

where M_ξ is the local streamwise Mach number. For certain cases, the retention of the term, $(1-\omega)\partial p/\partial \xi$, will lead to departure solutions. In the present study, this difficulty was encountered only at very high angles of attack and in these cases, the term was simply dropped.

The sublayer approximation method of Schiff and Steger utilizes the following step function in place of Eq. (19):

$$\omega = 1 \quad \text{if} \quad M_\xi > M^*$$

$$= 0 \quad \text{if} \quad M_\xi \le M^*$$

where M^* is a specified value near 1. Their method also removes the streamwise pressure gradient term from the energy equation in the sublayer region. To avoid departure solutions, Schiff and Steger suggest using a global iteration procedure.

In order to facilitate the application of the Vigneron technique Eq. (17) is rewritten as

$$\frac{\partial \bar{E}^*}{\partial \xi} + \frac{\partial \bar{P}}{\partial \xi} + \frac{\partial \bar{F}}{\partial \eta} + \frac{\partial \bar{G}}{\partial \zeta} = 0 \tag{20}$$

where

$$\bar{E} = \bar{E}^* + \bar{P} \tag{21}$$

and

$$\bar{E}^* = (1/J)(\xi_x E^* + \xi_y F^* + \xi_z G^*)$$

$$\bar{P} = (1/J)(\xi_x P_1 + \xi_y P_2 + \xi_z P_3)$$

$$E^* = E - P_1 \quad F^* = F - P_2 \quad G^* = G - P_3$$

$$P_1 = [0, (1-\omega)p, 0, 0, 0]^T \quad P_2 = [0, 0, (1-\omega)p, 0, 0]^T$$

$$P_3 = [0, 0, 0, (1-\omega)p, 0]^T \tag{22}$$

Numerical Solution of Equations

Grid Generation

At each ξ station, the computational domain [i.e., the (η,ζ) solution surface] is bounded by the bow shock and the body surface as seen in Fig. 1. For symmetrical flows, only one half of the computational domain needs to be considered since the other half is known from symmetry. The orientation of each (η,ζ) solution surface is purposely left arbitrary so that the optimum orientation can be selected for a given problem. In general, the optimum orientation occurs when the (η,ζ) solution surface is perpendicular to the local flow direction. The location of the grid points in each (η,ζ) solution surface is also left arbitrary so that the optimum distribution can be selected for a given problem. For the present study, the η lines are generated using straight rays which emanate from the NJ grid points situated along the body surface. The direction of each ray from a body grid point at (x_b, y_b, z_b) is given by the unit vector $\boldsymbol{n}$ which need not be a surface normal vector. Along each ray, NK grid points are positioned. These grid points are clustered near the wall in order to properly resolve the boundary layer. The length of each ray represents the shock standoff distance δ which is determined at each step from the shock boundary condition.

The generalized coordinates (ξ,η,ζ) are defined in such a way that at each ξ station, the (η,ζ) solution surface in the physical space is mapped into the shape of a unit square in the computational plane. The grid in the computational plane has uniform spacing in each direction given by

$$\Delta\eta = 1/(NK-1), \qquad \Delta\zeta = 1/(NJ-1) \tag{23}$$

so that $\eta = (k-1)\Delta\eta$ and $\zeta = (j-1)\Delta\zeta$. The physical and computational planes are related by the equations

$$x(j,k) = x_b(j) + \delta(j)s(k)[n(j)\cdot i]$$

$$y(j,k) = y_b(j) + \delta(j)s(k)[n(j)\cdot j]$$

$$z(j,k) = z_b(j) + \delta(j)s(k)[n(j)\cdot k] \tag{24}$$

where $s(k)$ is the stretching function

$$s(k) = 1 - \beta\left[\left(\frac{\beta+1}{\beta-1}\right)^\eta - 1\right] \Big/ \left[1+\left(\frac{\beta+1}{\beta-1}\right)^\eta\right] \tag{25}$$

which clusters more grid points near the wall ($\eta = 1$) as the stretching parameter β approaches one. The metrics x_η, y_η, z_η, x_ζ, y_ζ, z_ζ are computed numerically with central dif-

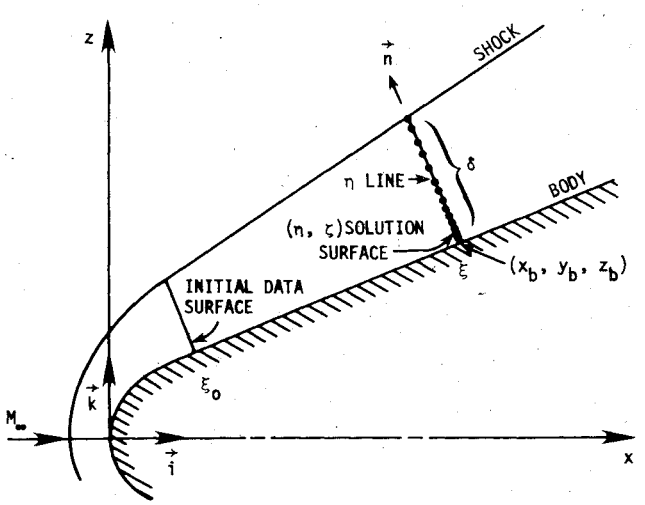

Fig. 1 Generation of grid.

ferences in the regularly spaced computational plane. The metrics x_ξ, y_ξ, z_ξ are evaluated with the aid of the expressions

$$x_\xi = (x_b)_\xi + \delta_\xi s(\boldsymbol{n}\cdot\boldsymbol{i}) + \delta s(\boldsymbol{n}\cdot\boldsymbol{i})_\xi$$

$$y_\xi = (y_b)_\xi + \delta_\xi s(\boldsymbol{n}\cdot\boldsymbol{j}) + \delta s(\boldsymbol{n}\cdot\boldsymbol{j})_\xi$$

$$z_\xi = (z_b)_\xi + \delta_\xi s(\boldsymbol{n}\cdot\boldsymbol{k}) + \delta s(\boldsymbol{n}\cdot\boldsymbol{k})_\xi \tag{26}$$

where $(x_b)_\xi$, $(y_b)_\xi$, $(z_b)_\xi$, $(\boldsymbol{n}\cdot\boldsymbol{i})_\xi$, $(\boldsymbol{n}\cdot\boldsymbol{j})_\xi$, $(\boldsymbol{n}\cdot\boldsymbol{k})_\xi$ are known from the body and grid geometry and δ_ξ is determined by the shock fitting procedure.

Finite-Difference Algorithm

Until recently, the PNS equations have been solved using iterative, implicit, finite-difference schemes. Vigneron et al.[4,15] were the first to employ a more efficient noniterative, implicit, approximate-factorization, finite-difference scheme to solve the PNS equations. This algorithm is a direct descendent of the schemes developed by Lindemuth and Killeen,[17] McDonald and Briley,[18] and Beam and Warming[19] to initially solve the unsteady Navier-Stokes equations. When applied to Eq. (20), the delta form of this algorithm is

$$\left[\frac{\partial \bar{E}^*}{\partial \bar{U}} + \frac{\theta_1}{1+\theta_2}\Delta\xi\frac{\partial}{\partial\zeta}\left(\frac{\partial \bar{G}}{\partial \bar{U}}\right)\right]\left(\frac{\partial \bar{E}^*}{\partial \bar{U}}\right)^{-1}$$

$$\times\left[\frac{\partial \bar{E}^*}{\partial \bar{U}} + \frac{\theta_1}{1+\theta_2}\Delta\xi\frac{\partial}{\partial\eta}\left(\frac{\partial \bar{F}}{\partial \bar{U}}\right)\right]\Delta^i\bar{U} = \frac{-\Delta\xi}{1+\theta_2}\left(\frac{\partial \bar{F}}{\partial\eta} + \frac{\partial \bar{G}}{\partial\zeta}\right)$$

$$+\frac{\theta_2}{1+\theta_2}\Delta^{i-1}\bar{E} - \Delta^i\bar{P} - \Delta\xi\left(\frac{\partial \bar{E}^*}{\partial\xi}\right)_{\bar{U}}^{i}$$

$$-\frac{\theta_1}{1+\theta_2}(\Delta\xi)^2\left[\frac{\partial}{\partial\eta}\left(\frac{\partial \bar{F}}{\partial\xi}\right)_{\bar{U}}^{i} + \frac{\partial}{\partial\zeta}\left(\frac{\partial \bar{G}}{\partial\xi}\right)_{\bar{U}}^{i}\right] \tag{27}$$

where superscript i refers to the station $\xi = i\Delta\xi$ and

$$\Delta^i\bar{U} = \bar{U}^{i+1} - \bar{U}^i \tag{28}$$

The terms $(\partial \bar{E}^*/\partial\xi)_{\bar{U}}^{i}$, $(\partial \bar{F}/\partial\xi)_{\bar{U}}^{i}$, and $(\partial \bar{G}/\partial\xi)_{\bar{U}}^{i}$ are evaluated with the aid of the expressions

$$\left(\frac{\partial \bar{E}^*}{\partial\xi}\right)_{\bar{U}} = \left(\frac{E^*}{J}\right)\frac{\partial\xi_x}{\partial\xi} + \left(\frac{F^*}{J}\right)\frac{\partial\xi_y}{\partial\xi} + \left(\frac{G^*}{J}\right)\frac{\partial\xi_z}{\partial\xi}$$

$$\left(\frac{\partial \bar{F}}{\partial\xi}\right)_{\bar{U}} = \left(\frac{E-E_v}{J}\right)\frac{\partial\eta_x}{\partial\xi} + \left(\frac{F-F_v}{J}\right)\frac{\partial\eta_y}{\partial\xi} + \left(\frac{G-G_v}{J}\right)\frac{\partial\eta_z}{\partial\xi}$$

$$\left(\frac{\partial \bar{G}}{\partial\xi}\right)_{\bar{U}} = \left(\frac{E-E_v}{J}\right)\frac{\partial\zeta_x}{\partial\xi} + \left(\frac{F-F_v}{J}\right)\frac{\partial\zeta_y}{\partial\xi} + \left(\frac{G-G_v}{J}\right)\frac{\partial\zeta_z}{\partial\xi} \tag{29}$$

where $(\,)_{\bar{U}}$ indicates $\bar{U}$ is held constant. The Jacobians $\partial\bar{F}/\partial\bar{U}$, $\partial\bar{G}/\partial\bar{U}$, and $\partial\bar{E}^*/\partial\bar{U}$ are given in Ref. 23. The partial derivatives $\partial/\partial\eta$ and $\partial/\partial\zeta$ are approximated by second-order accurate central differences.

For first-order accuracy in ξ, the Euler implicit scheme ($\theta_1 = 1$, $\theta_2 = 0$) is used. In this case, the Jacobians are evaluated at station i and the last term in brackets in Eq. (27) is dropped. Also, the explicit streamwise pressure gradient term $\Delta^i\bar{P}$ (which appears only in the sublayer region) is evaluated at a point outside the sublayer region using a first-order backward difference at station i. All of the results presented here were obtained with the Euler implicit scheme.

If second-order accuracy in ξ is desired, the three-point backward implicit scheme ($\theta_1 = 1$, $\theta_2 = \frac{1}{2}$) can be used. In this case, the Jacobians are evaluated at $i+\frac{1}{2}$ and the explicit streamwise pressure gradient term is evaluated at a point outside the sublayer region using a second-order backward difference at station i.

The algorithm given by Eq. (27) is implemented in the following manner

Step 1

$$\left[\frac{\partial \bar{E}^*}{\partial \bar{U}} + \frac{\theta_1}{1+\theta_2}\Delta\xi\frac{\partial}{\partial\zeta}\left(\frac{\partial \bar{G}}{\partial \bar{U}}\right)\right]\Delta\bar{U}_1 = \text{RHS [Eq. (27)]} \tag{30a}$$

Step 2

$$\Delta\bar{U}_2 = \frac{\partial \bar{E}^*}{\partial \bar{U}}\Delta\bar{U}_1 \tag{30b}$$

Step 3

$$\left[\frac{\partial \bar{E}^*}{\partial \bar{U}} + \frac{\theta_1}{1+\theta_2}\Delta\xi\frac{\partial}{\partial\eta}\left(\frac{\partial \bar{F}}{\partial \bar{U}}\right)\right]\Delta^i\bar{U} = \Delta\bar{U}_2 \tag{30c}$$

Step 4

$$\bar{U}^{i+1} = \bar{U}^i + \Delta^i\bar{U} \tag{30d}$$

In Eq. (30a), $\Delta\bar{U}_1$ represents all the remaining terms on the left-hand side of Eq. (27). Note that this procedure does not require the explicit evaluation of the matrix inverse $(\partial\bar{E}^*/\partial\bar{U})^{-1}$. Equations (30a) and (30c) represent block tridiagonal systems of equations that are solved using a routine written by Steger.[20] Also, artificial dissipation in the form of an explicit fourth-order smoothing term and an implicit second-order smoothing term has been added to the algorithm as described in Ref. 4.

Boundary Conditions

The flow conditions at the shock boundary are computed using the "shock fitting" technique developed by Thomas et al.[21] This procedure is described in Ref. 23. At the body surface, the normal pressure gradient is assumed zero. The velocity components are set equal to zero and the wall temperature is either specified for the case of an isothermal wall or is computed using a one-sided difference approximation for a zero normal temperature gradient when the wall is adiabatic. The density is then calculated using the equation of state. The flow conditions along $j = 1$ and $j = NJ$ are obtained by reflection about the planes of symmetry.

Initial Conditions

An initial data surface ($\xi = \xi_0$) is required to start a PNS calculation. The inviscid flow region of this initial data surface must be supersonic and the streamwise component of the velocity must be positive. For the blunt delta wing considered in the present study an axisymmetric, time-dependent, Navier-Stokes code[22] was used to compute the nose portion of the flowfield. The resulting axisymmetric solution was then recast in terms of the coordinates used in the PNS code to provide the three-dimensional starting data. The present use of an axisymmetric code to produce three-dimensional starting data was possible because the initial portion of the flow over a body with a spherical nosecap is axisymmetric about the wind axis provided that the spherical cap extends into the supersonic region of flow.[6] All of the cases considered in this study satisfy this criterion. In general, a three-dimensional Navier-Stokes code or a three-dimensional viscous shock layer code must be used to provide the initial data surface.

Results

The present generalized PNS code has been used to compute the laminar flow over a 70-deg sweep slab delta wing having a spherical nose and a cylindrical leading edge, see Fig. 2. The body shape and flow conditions were chosen to match the experiments of Bertram and Everhart.[12] These ex-

Table 1 Flow conditions

	$M_\infty = 6.8$	$M_\infty = 9.6$
$\tilde{p}_\infty$, N/m^2	889.2	130.3
$\tilde{T}_\infty$, K	60.2	47.5
Re_D	2.6×10^5	0.8×10^5
$\tilde{T}_{wall}$, K	317	317
γ	1.4	1.4
Pr	0.72	0.72

Table 2 Numerical cases

Case	M_∞	α, deg	Wall boundary condition	Grid ($NJ \times NK$)	β
1	6.8	0	Adiabatic	24×40	1.04
2	6.8	0	Isothermal	24×40	1.04
3	6.8	10	Adiabatic	24×40	1.04
4	9.6	0	Adiabatic	18×40	1.04
5	9.6	0	Isothermal	18×40	1.04
6	9.6	5	Isothermal	24×40	1.04
7	9.6	20	Adiabatic	25×40	1.04
8	9.6	41.5	Adiabatic	25×40	1.04

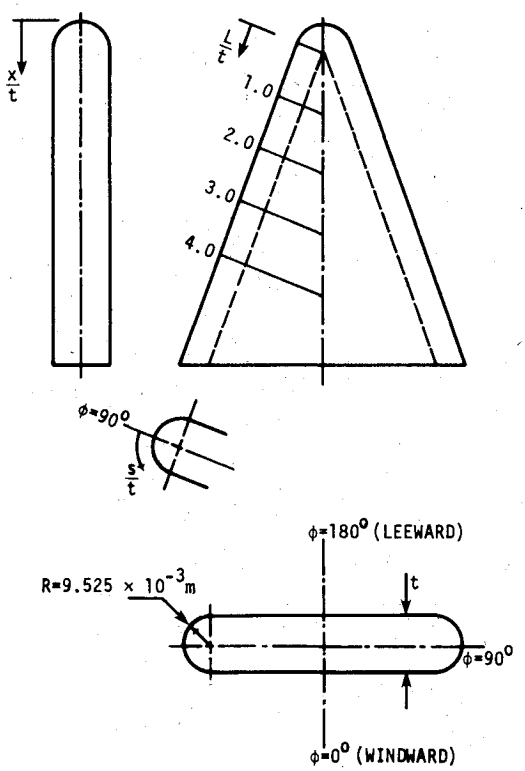

Fig. 2 Slab delta wing with 70-deg sweep.

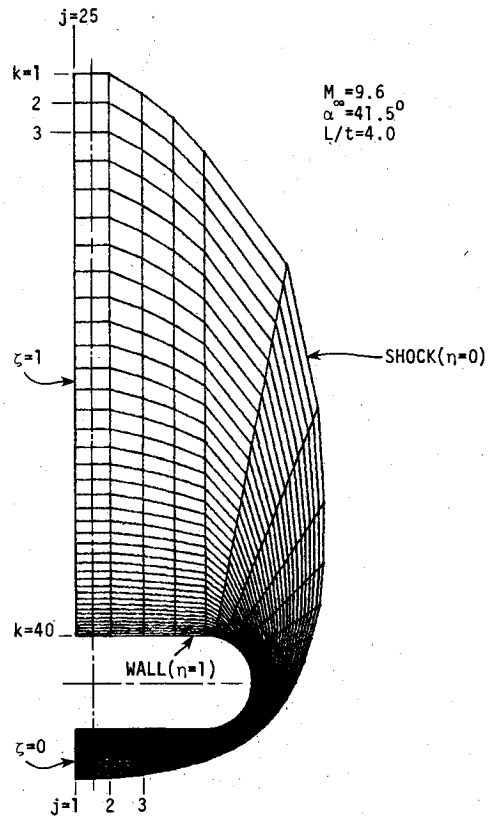

Fig. 3 Typical grid.

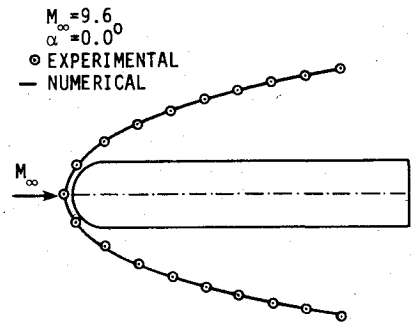

Fig. 4 Side view of shock shape (case 4).

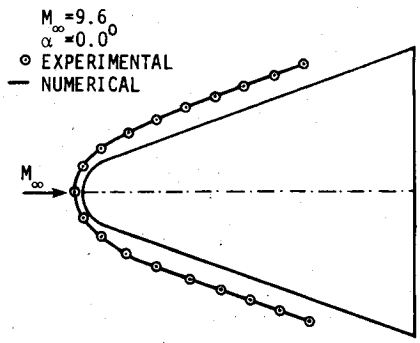

Fig. 5 Planform view of shock shape (case 4).

periments were conducted in the Langley 11-in. Hypersonic Tunnel at Mach numbers of 6.8 and 9.6 using air. The corresponding flow conditions are given in Table 1. In Table 1, $\tilde{T}_{wall}$ is the wall temperature for the heat transfer tests and Re_D is the freestream Reynolds number based on the nose diameter of 1.905×10^{-2} m. The angle of attack α was varied from -2.5 to $+45$ deg in the experimental tests.

A description of the numerical solutions is given in Table 2. In all the calculations, the (η, ζ) solution surfaces were constructed using rays that are normal to the body surface. Hence each (η, ζ) solution surface is a plane described by $L/t = \text{const}$ as seen in Fig. 2. The body grid points were distributed on the wing surface by placing an equal number on the top and bottom flat surfaces of the wing while the remainder were spaced equally around the leading edge. A typical grid is shown in Fig. 3. This grid is for the solution surface located at $L/t = 4.0$ in case 8 (see Table 2) and was drawn by a computer plotter using straight line segments between grid points.

The computed results are too numerous to show in their entirety in this paper. Instead, a representative sampling of

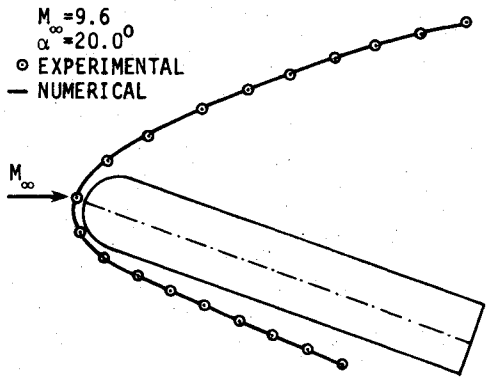

Fig. 6 Side view of shock shape (case 7).

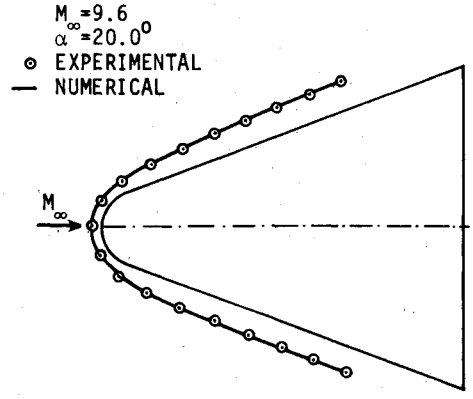

Fig. 7 Planform view of shock shape (case 7).

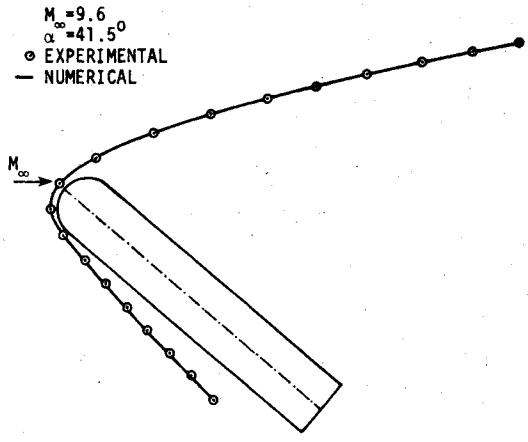

Fig. 8 Side view of shock shape (case 8).

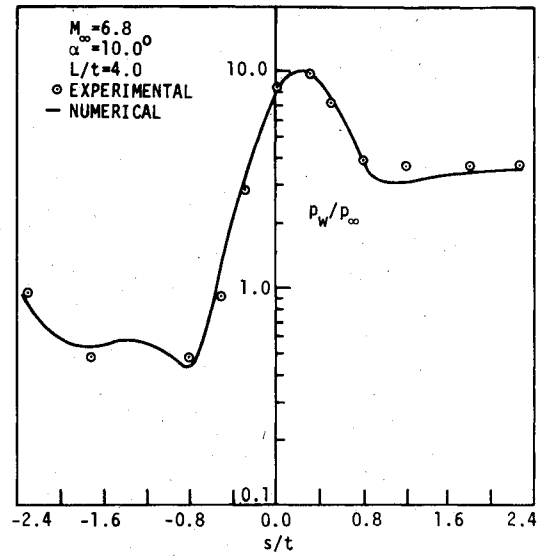

Fig. 9 Comparison of wall pressures (case 3).

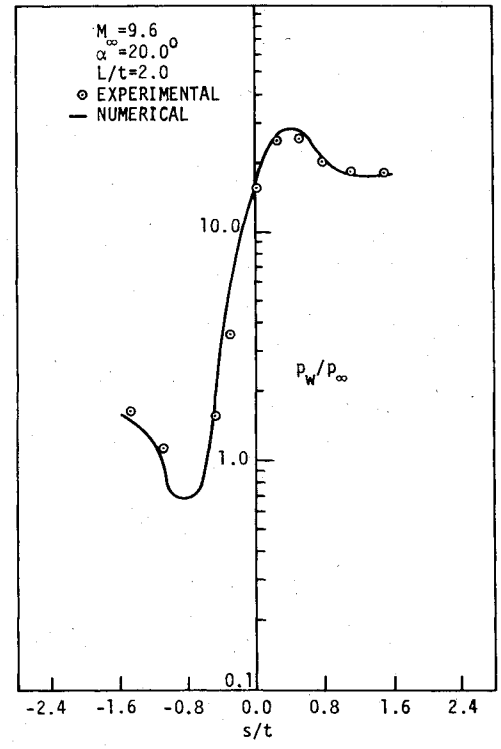

Fig. 10 Comparison of wall pressures (case 7).

the results is presented. The computed shock shapes for $M_\infty = 9.6$ at angles of attack of 0, 20, and 41.5 deg are shown in Figs. 4-8 along with the corresponding experimental shock shapes. Figures 4-7 show both the side and planform views of the shock at $\alpha = 0$ and 20 deg. Figure 8 shows the side view of the shock computed at $\alpha = 41.5$ deg and this is compared to the experimental shock shape obtained at $\alpha = 40$ deg. The corresponding planform view is not given since the experimental shock shape was distorted by tunnel-wall flow separation. In all cases, the computed shock shapes are in excellent agreement with the experimental results. Both the experiment and the present numerical study indicate that the shock shape is relatively insensitive to Mach number.

The wall pressures for several different cases are given in Figs. 9-11. These results were obtained with an adiabatic wall condition in order to match the experimental conditions. The wall pressures are plotted as functions of the nondimensionalized distance (s/t) which is measured along the body surface from the leading edge in a $L/t = \text{const}$ plane. The nondimensional distance (s/t) is positive on the windward side of the wing and is negative on the leeward side. Figure 9 shows the wall pressure at $L/t = 4.0$ for case 3; Fig. 10 shows the wall pressure at $L/t = 2.0$ for case 7; and Fig. 11 shows the wall pressure at $L/t = 4.0$ for case 8. In all the cases presented here, as well as for the cases not presented, the computed wall pressures are in good agreement with the experimental values.

Heat transfer coefficients are shown in Figs. 12 and 13. The heat transfer coefficients are normalized using the maximum heat transfer coefficient (h_{max}) in the given L/t plane. Figures 12 and 13 show the distributions at $L/t = 2.0$ and 3.0 for case 6. The computed heat transfer coefficients agree reasonably well with the experimental coefficients.

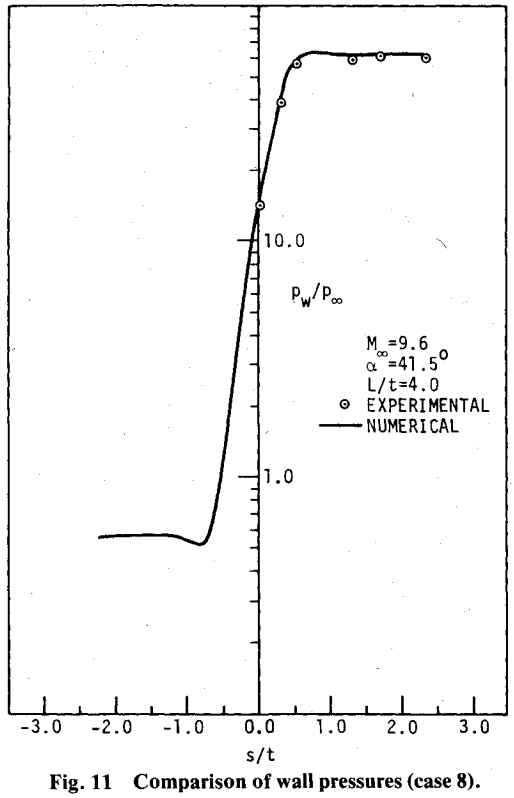

Fig. 11 Comparison of wall pressures (case 8).

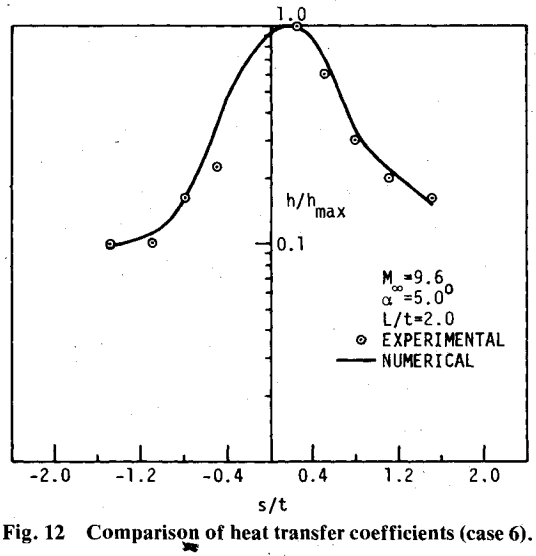

Fig. 12 Comparison of heat transfer coefficients (case 6).

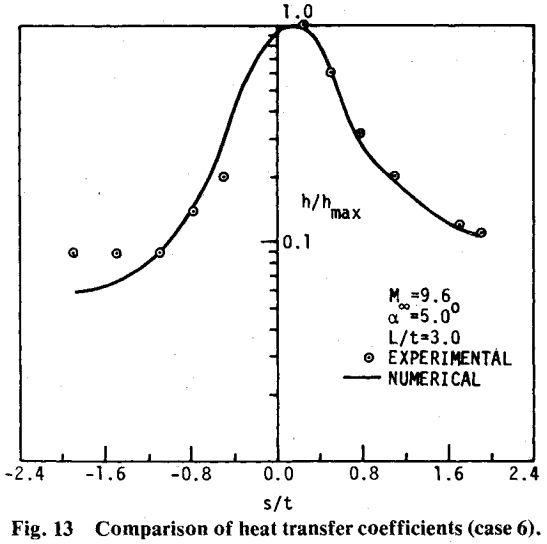

Fig. 13 Comparison of heat transfer coefficients (case 6).

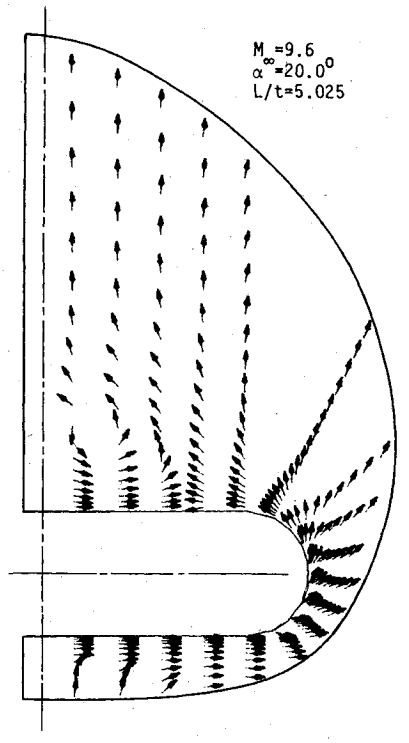

Fig. 14 Cross-flow velocity directions (case 7).

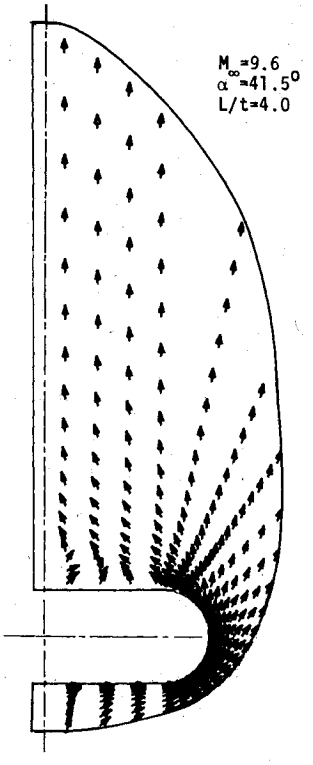

Fig. 15 Cross-flow velocity directions (case 8).

The Cartesian cross-flow velocity directions are shown in Fig. 14 for case 7 at $L/t = 5.025$. The primary vortex above the wing is clearly evident in this figure. Also, a small secondary vortex (not visible in Fig. 14) is discernable upon closer examination of the numerical results. Figure 15 shows the Cartesian cross-flow velocity directions for case 8 at $L/t = 4.0$. The primary vortex in this case appears to be located near the leeward side symmetry plane.

The results of this study were obtained on a CDC 7600 computer. The generalized PNS code required 1.06×10^{-3} s of computer time per step per grid point. A typical solution, such as case 8 (25×40 mesh), was obtained with 511 steps and 9 min of computer time.

Conclusions

A generalized PNS code has been developed to compute the steady supersonic viscous flow around arbitrary body shapes at high angles of attack. As a test, the code was used to calculate the laminar flow over a slab delta wing at angles of attack up to 41.5 deg and Mach numbers of 6.8 and 9.6. The excellent agreement of the present computational results with the experiments of Bertram and Everhart provides the necessary validation of the new code. Additional tests with more complex body shapes are now in progress to demonstrate the full generality of this code.

Acknowledgments

This work was supported by NASA Ames Research Center under Grant NGR 16-002-038 and the Engineering Research Institute, Iowa State University, Ames, Iowa. The authors which to acknowledge the contribution of Yvon C. Vigneron in developing the present technique for solving the PNS equations.

References

[1] Lin, T. C. and Rubin, S. G., "Viscous Flow Over a Cone at Moderate Incidence: I. Hypersonic Tip Region," *Computers and Fluids*, Vol. 1, Feb. 1973, pp. 37-57.

[2] Lubard, S. C. and Helliwell, W.S., "Calculation of the Flow on a Cone at High Angle of Attack," *AIAA Journal*, Vol. 12, July 1974, pp. 965-974.

[3] Helliwell, W. S. and Lubard, S. C., "An Implicit Method for Three-Dimensional Viscous Flow with Application to Cones at Angle of Attack," *Computers and Fluids*, Vol. 3, No. 1, 1975, pp. 83-101.

[4] Vigneron, Y. C., Rakich, J. V., and Tannehill, J. C., "Calculation of Supersonic Viscous Flow over Delta Wings with Sharp Subsonic Leading Edges," AIAA Paper 78-1137, July 1978.

[5] Lin, T. C. and Rubin, S. G., "A Numerical Model for Supersonic Viscous Flow Over a Slender Reentry Vehicle," AIAA Paper 79-0205, Jan. 1979.

[6] Lubard, S. C. and Rakich, J. V., "Calculation of the Flow on a Blunted Cone at a High Angle of Attack," AIAA Paper 75-149, Jan. 1975.

[7] Rakich, J. V. and Lubard, S. C., "Numerical Computation of Viscous Flows on the Lee Side of Blunt Shapes Flying at Supersonic Speeds," *Proceedings NASA Conference on Aerodynamic Analyses Requiring Advanced Computers*, NASA SP-347, March 1975, pp. 531-542.

[8] Schiff, L. B. and Steger, J. L., "Numerical Simulation of Steady Supersonic Viscous Flow," AIAA Paper 79-0130, Jan. 1979.

[9] Rakich, J. V., Vigneron, Y. C., and Agarwal, R., "Computation of Supersonic Viscous Flows Over Ogive-Cylinders at Angle of Attack," AIAA Paper 79-0131, Jan. 1979.

[10] Schiff, L. B. and Sturek, W. B., "Numerical Simulation of Steady Supersonic Flow Over an Ogive-Cylinder-Boattail Body," AIAA Paper 80-0066, Jan. 1980.

[11] Helliwell, W. S., Dickinson, R. P., and Lubard, S. C., "Viscous Flow Over Arbitrary Geometries at High Angle of Attack," AIAA Paper 80-0064, Jan. 1980.

[12] Bertram, M. H. and Everhart, P. E., "An Experimental Study of the Pressure and Heat Transfer Distribution on a 70° Sweep Slab Delta Wing in Hypersonic Flow," NASA TR R-153, Dec. 1963.

[13] Viviand, H., "Conservative Forms of Gas Dynamic Equations," *La Recherche Aerospatiale*, No. 1, Jan.-Feb. 1974, pp. 65-68.

[14] Lighthill, M. J., "On Boundary Layers and Upstream Influence. II. Supersonic Flows Without Separation," *Proceedings of the Royal Society, Series A*, Vol. 217, 1953.

[15] Vigneron, Y. C., Rakich, J. V., and Tannehill, J. C., "Calculation of Supersonic Viscous Flow over Delta Wings with Sharp Subsonic Leading Edges," NASA TM-78500, June 1978.

[16] Rubin, S. G. and Lin, T. C., "Numerical Methods for Two- and Three-Dimensional Viscous Flow Problems: Application to Hypersonic Leading Edge Equations," PIBAL Rept. 71-8, Polytechnic Institute of Brooklyn, Farmingdale, N.Y., April 1971.

[17] Lindemuth, I. and Killeen, J., "Alternating Direction Implicit Techniques for Two Dimensional Magnetohydrodynamics Calculations," *Journal of Computational Physics*, Vol. 13, Oct. 1973, pp. 181-208.

[18] McDonald, H. and Briley, W. R., "Three-Dimensional Supersonic Flow of a Viscous or Inviscid Gas," *Journal of Computational Physics*, Vol. 19, Oct. 1975, pp. 150-178.

[19] Beam, R. and Warming, R. F., "An Implicit Factored Scheme for the Compressible Navier-Stokes Equations," *AIAA Journal*, Vol. 16, April 1978, pp. 393-401.

[20] Steger, J. L., "Implicit Finite-Difference Simulation of Flow About Arbitrary Geometries with Application to Airfoils," AIAA Paper 77-665, June 1977.

[21] Thomas, P. D., Vinokur, M., Bastianon, R. A., and Conti, R. J., "Numerical Solution for Three-Dimensional Inviscid Supersonic Flows," *AIAA Journal*, Vol. 10, July 1972, pp. 887-894.

[22] Tannehill, J. C., Holst, T. L., and Rakich, J. V., "Numerical Computation of Two-Dimensional Viscous Blunt Body Flows with an Impinging Shock," *AIAA Journal*, Vol. 4, Feb. 1976, pp. 204-211.

[23] Tannehill, J. C., Venkatapathy, E., and Rakich, J. V., "Numerical Solution of Supersonic Viscous Flow over Blunt Delta Wings," AIAA Paper 81-0049, Jan. 1981.